

## Self-Assembly

International Edition: DOI: 10.1002/anie.201916149  
 German Edition: DOI: 10.1002/ange.201916149

# Magnifying the Structural Components of Biomembranes: A Prototype for the Study of the Self-Assembly of Giant Lipids

Xiao-Yun Yan, Zhiwei Lin,\* Wei Zhang, Hui Xu, Qing-Yun Guo, Yuchu Liu, Jiancheng Luo, Xian-You Liu, Rongchun Zhang, Jiahao Huang, Tong Liu, Zebin Su, Ruimeng Zhang, Shuailin Zhang, Tianbo Liu, and Stephen Z. D. Cheng\*

**Abstract:** How biomembranes are self-organized to perform their functions remains a pivotal issue in biological and chemical science. Understanding the self-assembly principles of lipid-like molecules hence becomes crucial. Herein, we report the mesostructural evolution of amphiphilic sphere-rod conjugates (giant lipids), and study the roles of geometric parameters (head-tail ratio and cross-sectional area) during this course. As a prototype system, giant lipids resemble natural lipidic molecules by capturing their essential features. The self-assembly behavior of two categories of giant lipids (I-shape and T-shape, a total of 8 molecules) is demonstrated. A rich variety of mesostructures is constructed in solution state and their molecular packing models are rationally understood. Giant lipids recast the phase behavior of natural lipids to a certain degree and the abundant self-assembled morphologies reveal distinct physiochemical behaviors when geometric parameters deviate from natural analogues.

## Introduction

For decades, researchers have made great efforts to replicate, modify, and improve the properties and functions of living biological membranes.<sup>[1]</sup> One significant advance is adopting the “scale-up” strategies by using magnified analogues of natural lipids to generate liposome-like nanostructures (Figure 1 a). The increased membrane thickness endows better impermeability,<sup>[2]</sup> mechanical strength,<sup>[3]</sup> feasibility for chemical modification,<sup>[4]</sup> and ability to incorporate pore-forming proteins.<sup>[5]</sup> In this regard, amphiphilic block copolymers,<sup>[6]</sup> Janus dendrimers,<sup>[5b,7]</sup> giant surfactants,<sup>[8]</sup> proteins,<sup>[9]</sup> colloidal particles,<sup>[10]</sup> and others<sup>[11]</sup> have revolutionized fundamental understanding of the scope and limitations of

molecular architecture while self-assembling.<sup>[12]</sup> These advances further fuel countless innovations in smart nano-carriers,<sup>[13]</sup> in vivo imaging vehicles,<sup>[14]</sup> or artificial organelles.<sup>[15]</sup> Though chosen by nature, lipid-type geometry itself, with one head and two extended tails, has rarely been studied in a magnified size, which necessitates the design and investigation of a prototype system.

When one designs a structurally magnified analogue of natural lipids and studies their self-assembly, three essential issues need to be considered: head-tail configuration, molecular weight distribution, and chain interpenetration (Figure 1b). A hydrophilic head tethered by hydrophobic tails is an essential feature of natural lipids. Considering the low degree of freedom, modelling natural lipids as shape-persistent rod-like motifs has become a widely applied approach.<sup>[16]</sup> It is therefore imperative to render enlarged analogues with relatively rigid conformation to better capture the head-tail feature. Secondly, molecular weight distribution is associated with the composition of molecules. Structural components of biomembranes (like phospholipids or glycolipids) bear precise stereochemistry and monodispersed molecular mass, which, however, are notoriously formidable to realize in block copolymers. Thirdly, membrane-forming natural lipids are in a liquid-crystalline state at room temperature.<sup>[17]</sup> Acyl chains therefore are fully extended without other chain conformations and interpenetration, which is challenging for magnified analogues, with flexible conformations, to mimic.<sup>[18]</sup> In our previous work, we systematically explored the self-assembly behaviors of giant surfactants composed of a hydrophilic head tethered with hydrophobic polymer chains.<sup>[19]</sup> Though head-tail geometries were constructed and hydrophobic chains were found to be rather stretched when forming micelles, it is of significant interest to establish a prototype of giant lipids with tunable topologies, rigid chain conformations, monodispersed molecular weights and stereochemistry.

Our major focus is on the physiochemical principles when lipids are magnified to “giant lipids”. To this end, we magnify the scale of natural lipids while retaining their topological features. We simplify a lipidic molecule as one spherical hydrophilic head tethered by two rod-like hydrophobic tails, and reconstruct the sphere-rod geometry following this blueprint. The “molecular lego” approach, which emphasizes topologically precise synthesis and assembly, becomes a powerful tool to achieve this goal.<sup>[20]</sup> Among the geometric motifs developed by our group<sup>[21]</sup> and others,<sup>[11c,22]</sup> we choose hydrophilic C<sub>60</sub> derivatives as a head and hydrophobic conjugated oligomers as tails to build giant lipids. Two geometric

[\*] X.-Y. Yan, Prof. W. Zhang, X.-Y. Liu, Prof. R.-C. Zhang,

Prof. S. Z. D. Cheng

South China Advanced Institute for Soft Matter Science and Technology, School of Molecular Science and Engineering, South China University of Technology, Guangzhou 510640 (China)

X.-Y. Yan, Dr. Z. Lin, H. Xu, Q.-Y. Guo, Y. Liu, J. Luo, J. Huang, T. Liu, Z. Su, R.-M. Zhang, S. Zhang, Prof. T.-B. Liu, Prof. S. Z. D. Cheng

Department of Polymer Science, College of Polymer Science and Polymer Engineering, The University of Akron, Akron, OH 44325-3909 (USA)

E-mail: zl21@zips.uakron.edu

scheng@uakron.edu

 Supporting information and the ORCID identification number(s) for the author(s) of this article can be found under:

<https://doi.org/10.1002/anie.201916149>.

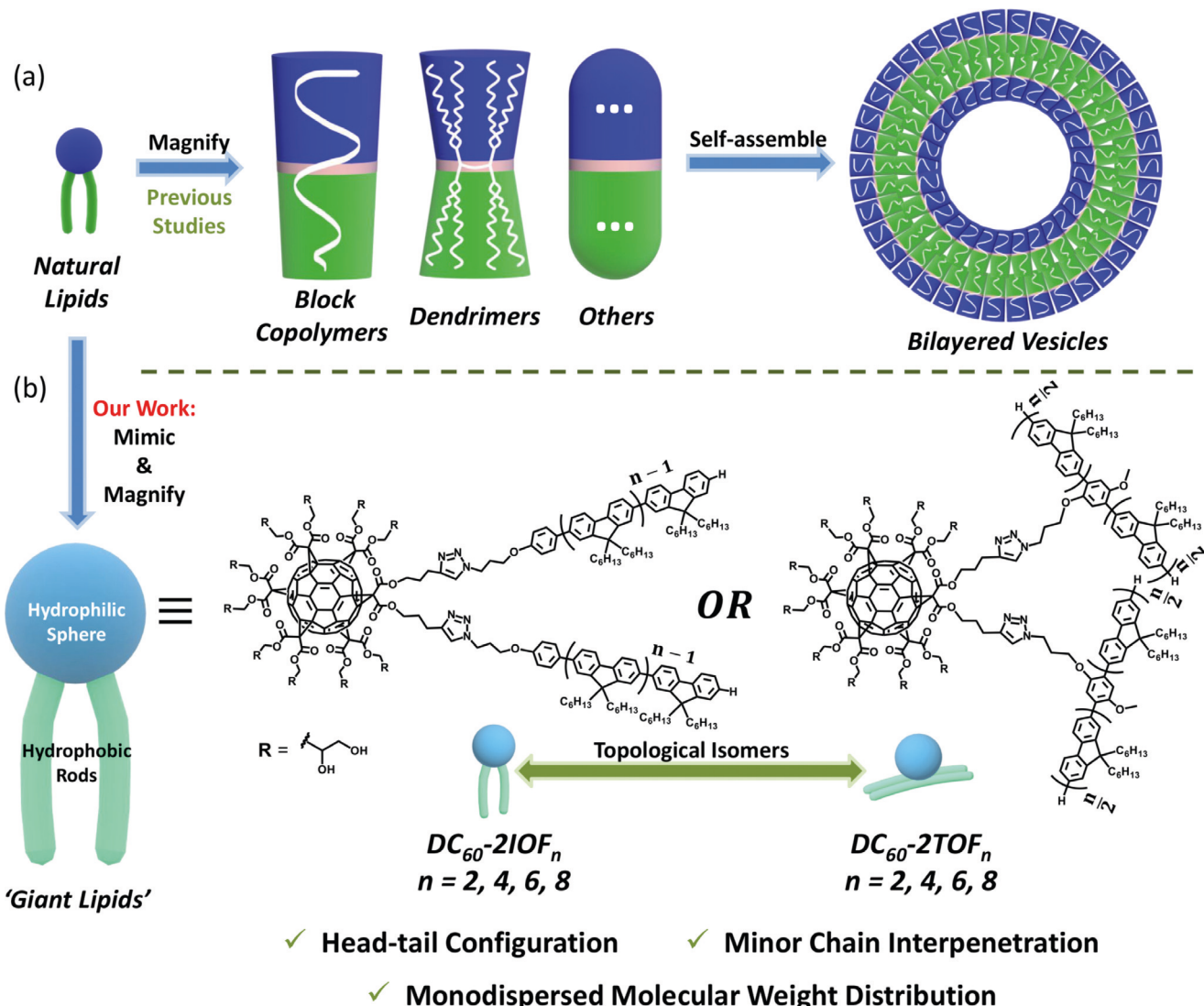


**Figure 1.** a) Reported "scale-up" strategies to construct liposome-like nanostructures. b) Illustration of shape-mimicking giant lipids and their molecular structures. Chemical structures and models of the linear I-shape series and branched T-shape series are illustrated. DC<sub>60</sub>: blue spheres, OF: cyan rods. (Due to the hydrophilic nature of triazole rings and ester groups,<sup>[23]</sup> we attribute the soft linkers to the spherical DC<sub>60</sub> part.)

parameters that fundamentally dictate self-assembly, including the ratio of the length of head and tail (referred to as head-tail ratio) and the lateral area of hydrophobic tails facing towards the hydrophilic head (referred to as cross-sectional area), are precisely manipulated during this course (Supporting Information, Discussion 1.1). To investigate the underlying physicochemical rules over a broader range, the values of geometric parameters tested span from the naturally occurred lipids to those inaccessible to living cells or organelles (Supporting Information, Table S1). More importantly, they fully address the aforementioned three issues through their rod-like shape with less variable conformations, precise but tunable chemical structures, and liquid-crystalline behavior with minor chain interpenetration.

## Results and Discussion

### Molecular Design

In our previous work, we demonstrated the synthesis, solid-state phase behaviors, and semiconducting properties of sphere-rod conjugates.<sup>[24]</sup> In this contribution, we focus on the solution self-assembly behaviors of sphere-rod conjugates, which are referred to as giant lipids. They bear one head of hydroxyl-functionalized C<sub>60</sub> (DC<sub>60</sub>) and two tails of oligofluorene (OF) rods. Both subunits are shape-persistent (DC<sub>60</sub> is essentially a spherical motif and OF could be regarded as a rigid rod) and the amphiphilicity endows sufficient incompatibility in the following self-assembly stage. Giant lipids in this study are divided into two categories based on the tethering point between DC<sub>60</sub> and OF tails (referred to as I- or T-shape, respectively, Figure 1b). In the I-shape series, the

tethering point is placed at the terminus of the OF tails (Figure 1b,  $DC_{60}\text{-2IOF}_n$ ), while in the T-shape series, it is located at the midpoint of the OF tails (Figure 1b,  $DC_{60}\text{-2TOF}_n$ ). With the same number of fluorenes ( $n_f$ ), the I-shape and T-shape giant lipids possess an identical composition but distinct molecular topologies, and they are thus regarded as topological isomers. Furthermore, the fluorene number can be tuned to afford various OF tail lengths, which, together with the changeable molecular topology, enables the precise manipulation of the aforementioned head-tail ratio and cross-sectional area. In our study, I-shape and T-shape molecules are specifically designed to evaluate the geometric effects in linear and branched lipids, respectively, for their pivotal roles in building biomembranes.

#### Self-Assembly Behavior of the I-Shape Series

I-shape molecules are designed with variant head-tail ratios to mimic the linear lipids with varying length of hydrocarbon tails. We first investigated the self-assembly behavior of giant lipids with short tail lengths ( $DC_{60}\text{-2IOF}_2$  and  $DC_{60}\text{-2IOF}_4$ ). Air-dried samples from prepared solutions (sample preparation is described in the Experimental Section in the Supporting Information) were examined by bright-field transmission electron microscopy (TEM), and typical vesicular morphologies were observed for  $DC_{60}\text{-2IOF}_2$  (Figure 2a). A round-shaped morphology with homogeneous electron density was observed for  $DC_{60}\text{-2IOF}_4$  (Figure 2b). Gray value analysis of merged edges reveals a four-layered structure in agreement with a vesicular instead of coin-type

structure (Supporting Information, Figure S1c,d).<sup>[8a]</sup> Cryo-TEM of  $DC_{60}\text{-2IOF}_4$  indicates the non-spherical shape and wrinkled surface texture (Supporting Information, Figure S2), which rules out the existence of multi-layered “onion” vesicles.<sup>[25]</sup> The vesicular structures of  $DC_{60}\text{-2IOF}_2$  and  $DC_{60}\text{-2IOF}_4$  were further verified by CONTIN analysis of dynamic light scattering (DLS) measurements (Figure 3a and Supporting Information, Figure S3a). The hydrodynamic radius ( $R_h$ ) of assemblies for  $DC_{60}\text{-2IOF}_4$  (96 nm, Figure 3a) at all scattering angles agrees with the vesicle size observed by TEM imaging (Figure 2b, approximately 200 nm in average diameter). Such angular independence characteristics tally with the isotropic vesicular morphology, otherwise morphological anisotropy in solution would give variant  $R_h$  at different scattering angles.<sup>[26]</sup> When the tail length of giant lipids is increased to  $DC_{60}\text{-2IOF}_6$  and  $DC_{60}\text{-2IOF}_8$ , two-dimensional (2D) nanosheets with a flat surface were observed (Figure 2c,d). Self-assembly at a slower rate suggests that the 2D nanosheet is the thermodynamically favored morphology for  $DC_{60}\text{-2IOF}_8$  (Supporting Information, Figure S4c and Discussion 1.2). In contrast to vesicles, the  $R_h$  values of 2D nanosheets vary with scattering angles (Figure 3a and Supporting Information, Figure S3b), which is consistent with scattering feature of anisotropic assembled structures in solution.<sup>[27]</sup>

To understand the packing mode at the molecular level, we performed atomic force microscopy (AFM) to measure the thicknesses of assemblies. AFM images reveal dispersed vesicles and 2D nanosheets with uniform thicknesses for  $DC_{60}\text{-2IOF}_4$  and  $DC_{60}\text{-2IOF}_6$ , (Figure 3b,c), respectively, in good agreement with our TEM observations (Figure 2c and Supporting Information, Figure S1a). After solvent evaporation, the vesicles of  $DC_{60}\text{-2IOF}_4$  are expected to collapse and the thickness of these vesicles is 21.1 nm according to the AFM height profile (Figure 3d, top). Scale measurement of zoom-in TEM images gives a very close thickness of 22.2 nm (Supporting Information, Figure S1b). Two-staged packing with doubled thickness at the boundary of the dried assembly was also measured for further verification (Supporting Information, Figure S5a–c). Considering the diameter of  $DC_{60}$  is about 1.3 nm (Supporting Information, Discussion 1.3) and the simulated rod length of  $\text{IOF}_4$  is 3.63 nm (Supporting Information, Figure S6a), it is suggested that the as-formed vesicles possess a double-layered molecular packing, as illustrated in inset iii of Figure 3e. On the other hand, the thickness of 2D nanosheets is measured to be 7.9 nm, which is approximately the thickness of two layers of  $DC_{60}$  plus one layer of  $\text{IOF}_6$  (rod length is 5.30 nm, Supporting Information, Figure S6a). The stacked thickness of two layers was also measured for further verification (Supporting Information, Figure S5d–f). Thus, we speculate that the 2D nanosheets are constructed by two  $DC_{60}$  layers on the top and bottom with interdigitated rods sandwiched in between (inset iv in Figure 3e). AFM measurements suggest a similar bilayered model for shorter-rod  $DC_{60}\text{-2IOF}_2$  (Supporting Information, Figure S7a–c) and an interdigitated model for longer-rod  $DC_{60}\text{-2IOF}_8$  (Supporting Information, Figure S7d–f). It is very interesting to note that the double-layered molecular packing of vesicles is consistent with our previous

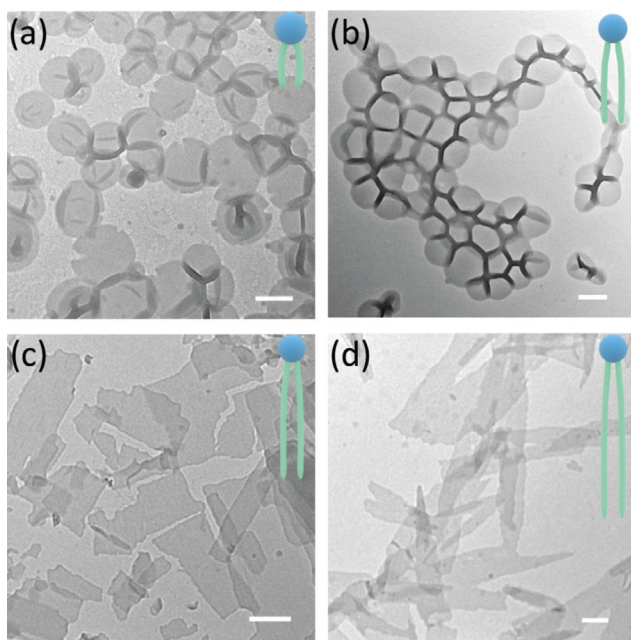


**Figure 2.** Bright-field TEM images of a)  $DC_{60}\text{-2IOF}_2$ , b)  $DC_{60}\text{-2IOF}_4$ , c)  $DC_{60}\text{-2IOF}_6$ , and d)  $DC_{60}\text{-2IOF}_8$ . Upper-right insets are the corresponding molecular models, whose head-tail ratios are estimated based on the calculation (Supporting Information, Table S1). Scale bar: 200 nm (a–d).  $DC_{60}$ : blue spheres, OF: cyan rods.

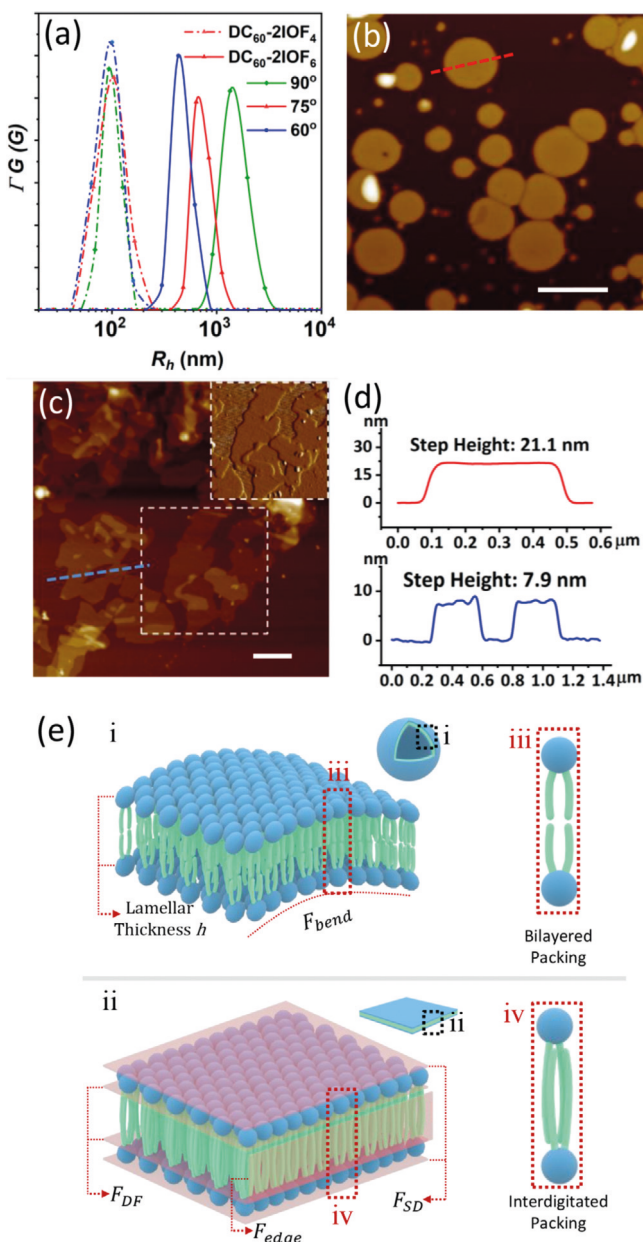


**Figure 3.** Morphological characterization of I-shape giant lipids. a) DLS profile of DC<sub>60</sub>-2IOF<sub>4</sub> (dashed line) and DC<sub>60</sub>-2IOF<sub>6</sub> (solid line). b) AFM image of DC<sub>60</sub>-2IOF<sub>4</sub> in the height mode. c) AFM image of DC<sub>60</sub>-2IOF<sub>6</sub> in the height mode. The upper-right inset is the amplitude image in the selected area (outlined by a white dashed square). d) Height profile of DC<sub>60</sub>-2IOF<sub>4</sub> (top, red dashed line in panel b) and DC<sub>60</sub>-2IOF<sub>6</sub> (bottom, blue dashed line in panel c). e) Morphological evolution from vesicle to nanosheet. The insets i and ii indicate a curved, bilayered packing model and a flat, interdigitated packing model, respectively. Key parameters regarding the corresponding free energy discussion are labeled. The insets iii and iv illustrate the detailed molecular packing modes. Dashed squares outline the selected regions of corresponding insets (DC<sub>60</sub>: blue spheres, OF: cyan rods). Scale bar: 500 nm (b, c).

experimental observations in the bulk;<sup>[24]</sup> however, the interdigitated molecular packing in 2D nanosheets was not observed in the bulk.

To further understand the origin of the diverse assembled structures, we assess the morphological evolution from a thermodynamic perspective by qualitatively incorporating various contributions of free energy. Two major parameters are associated with the transition from bilayered vesicles to interdigitated nanosheets by changing the number of fluorenes ( $n_f$ ): 1) bending energy associated with the deformational penalty of an elastic membrane ( $F_{\text{bend}}$ , inset i in Figure 3e) and 2) interfacial energy originating from the enhanced hydrophilic/hydrophobic effects between two immiscible components ( $F_{\text{interface}}$ , including all energetic terms in inset ii in Figure 3e).<sup>[28]</sup> On the basis of the Helfrich model, for a spherical vesicle,  $F_{\text{bend}}$  is characterized as [Eq. (1)]:

$$F_{\text{bend}} = 8\pi\kappa \quad (1)$$

where  $\kappa$  is the bending modulus.<sup>[29]</sup> From a mechanical perspective, the spontaneous curvature produced during vesicle formation is closely related with the bending modulus  $\kappa$ , which is expressed by  $\kappa \approx h^2$  (Supporting Information, Discussion 1.4),<sup>[30]</sup> where  $h$  is the thickness of lamellae (inset i in Figure 3e). Since hydrophobic tails stand perpendicular to the lamellar plain,  $\kappa$  increases with the length of OF, which results in a higher  $F_{\text{bend}}$  and prevents the formation of curved structure.  $F_{\text{interface}}$  can be broken down into three contributions resulting from all interfacial areas involved [Eq. (2)]:

$$F_{\text{interface}} = F_{\text{SD}} + F_{\text{DF}} + F_{\text{edge}} \quad (2)$$

where  $F_{\text{SD}}$ ,  $F_{\text{DF}}$  and  $F_{\text{edge}}$  are free energy contributed by the dissociation of homogenous phase and creation of heterogeneous interfacial areas between solvent/DC<sub>60</sub>, DC<sub>60</sub>/OF, and OF/solvent, respectively (inset ii in Figure 3e).<sup>[31]</sup> To minimize  $F_{\text{SD}}$  and  $F_{\text{DF}}$  the hydrophilic DC<sub>60</sub> are forced to point towards the polar solvents. To lower  $F_{\text{edge}}$ , a flat, layered structure tends to bend and close up to minimize the edge area where OF tails are fully exposed.<sup>[32]</sup> Interfacial free energy originating from two immiscible components (denoted as  $a$  and  $b$ ) can be estimated by  $F_{ab} \approx \gamma_{ab} S_{ab} \approx \sqrt{\chi_{ab}} S_{ab}$ , where  $\chi_{ab}$  is the Flory–Huggins parameter,  $\gamma_{ab}$  is the interfacial tension, and  $S_{ab}$  is the interfacial area.<sup>[33]</sup> Considering  $\chi_{edge}$  between OF and a poor solvent is estimated to be an order of magnitude larger than  $\chi_{SD}$  and  $\chi_{DF}$ <sup>[34]</sup> where  $\chi_{edge}$ ,  $\chi_{SD}$ , and  $\chi_{DF}$  are the Flory–Huggins parameters originating from OF/solvent, solvent/DC<sub>60</sub>, and DC<sub>60</sub>/OF interfaces, respectively,  $F_{\text{edge}}$  is expected to have major contributions to  $F_{\text{interface}}$ , compared with  $F_{\text{SD}}$  and  $F_{\text{DF}}$ . Therefore, a delicate balance between  $F_{\text{bend}}$  and  $F_{\text{edge}}$  determines the final self-assembling morphologies.

In the I-shape series, when the tails are short ( $h$  is small in DC<sub>60</sub>-2IOF<sub>2</sub> and DC<sub>60</sub>-2IOF<sub>4</sub>), the  $F_{\text{bend}}$  is relatively low, and  $F_{\text{interface}}$  will dominate the assembled structure formation. Thus, bilayered vesicles are formed to minimize  $F_{\text{edge}}$ . With the increase of OF rod length,  $F_{\text{bend}}$  increases more significantly than  $F_{\text{edge}}$ , as the former is associated with  $h^2$ , while the latter is linearly proportional to  $h$  ( $S_{\text{edge}} \approx h$ ). As a result,  $F_{\text{bend}}$  becomes a dominating factor. To minimize  $F_{\text{bend}}$ , the 2D nanosheets without bending curvature are yielded for DC<sub>60</sub>-2IOF<sub>6</sub> and DC<sub>60</sub>-2IOF<sub>8</sub>. Meanwhile, in order to lower  $F_{\text{edge}}$

and further stabilize the 2D nanosheets, an interdigitated molecular packing within 2D nanosheets is adapted. Though the interdigitated molecular packing may increase  $F_{SD}$  and  $F_{DF}$  this free energy penalty can be compensated by the decreased  $F_{edge}$ , given its dominating contribution in  $F_{interface}$ .

### Self-Assembly Behavior of the T-Shape Series

T-shape molecules are designed with varying cross-sectional areas to mimic the branched lipids with varying number of hydrocarbon tails. Despite the identical compositions, T-shape giant lipids exhibit completely distinct self-assembly

behaviors from their I-shape topological isomers.  $DC_{60}$ -2TOF<sub>2</sub> self-assembles into vesicles as revealed by TEM and DLS (Figure 4a and Supporting Information, Figure S8a). The AFM height profile suggests a bilayered molecular packing in which the rod-part would tilt up towards  $DC_{60}$  (Figure 4e). Increasing the tail length to  $DC_{60}$ -2TOF<sub>4</sub> and  $DC_{60}$ -2TOF<sub>6</sub> results in the formation of colloid particles (Figure 4b,c). As indicated by DLS, constant  $R_h$  values verify the isotropic features of self-assembled colloids (Supporting Information, Figure S8b,c). After being stained with RuO<sub>4</sub> vapor for 10 minutes, a zoom-in TEM image of colloidal particles of  $DC_{60}$ -2TOF<sub>4</sub> exhibits both hexagonal and lamellar patterns (Figure 4f and Supporting Information, Figure S9a–

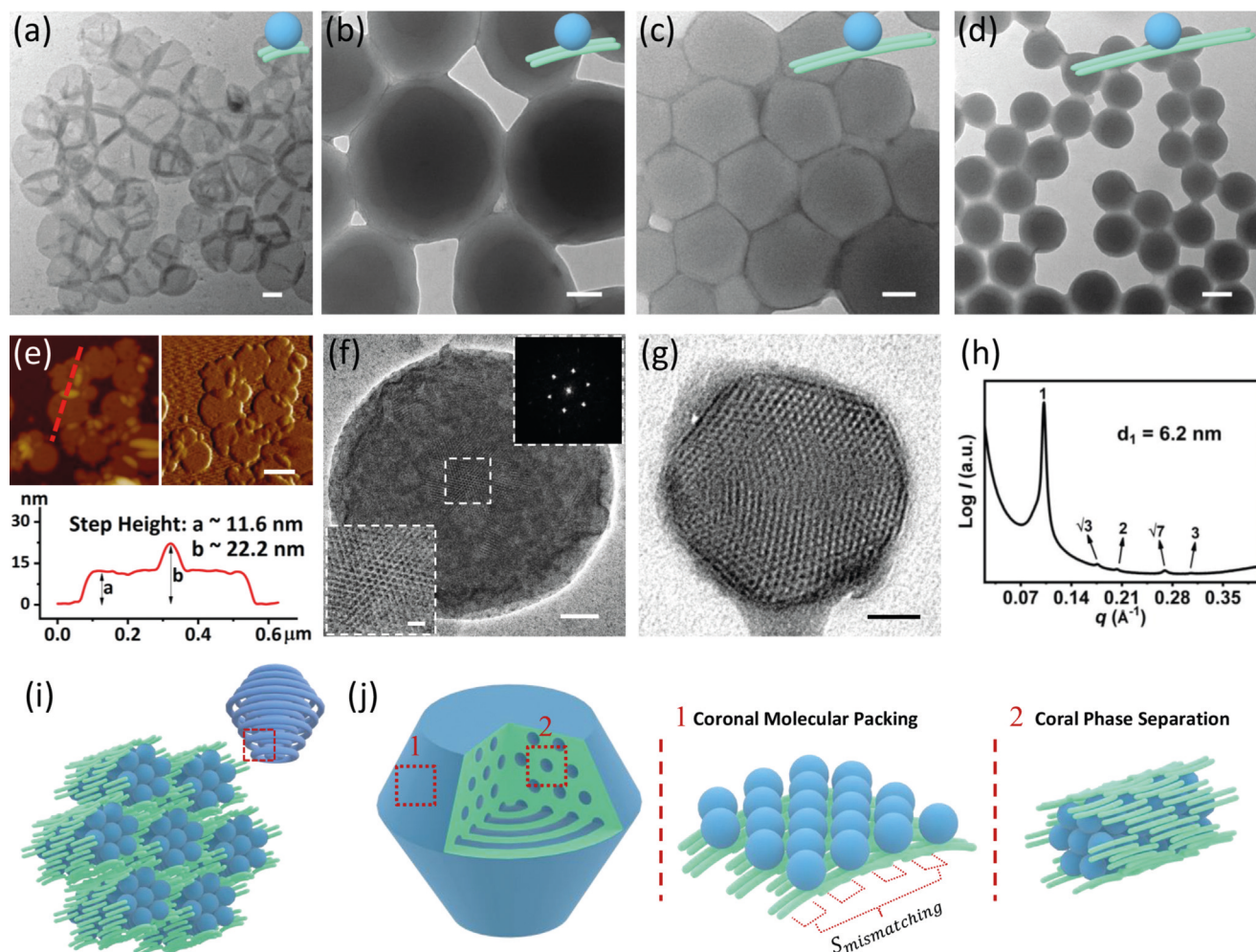


**Figure 4.** Morphological characterization of T-shape giant lipids. Bright-field TEM images of a)  $DC_{60}$ -2TOF<sub>2</sub>, b)  $DC_{60}$ -2TOF<sub>4</sub>, c)  $DC_{60}$ -2TOF<sub>6</sub>, and d)  $DC_{60}$ -2TOF<sub>8</sub>. Upper-right insets are the corresponding molecular models, whose head-tail ratios are estimated based on the calculation (Supporting Information, Table S1;  $DC_{60}$ : blue spheres, OF: cyan rods). e) AFM image of  $DC_{60}$ -2TOF<sub>2</sub> in the height mode (upper-left) and in the amplitude mode (upper-right). The height profile (bottom) is denoted by a dashed line in Figure 4e. f) Zoom-in TEM image of a  $DC_{60}$ -2TOF<sub>4</sub> colloidal particle (stained with RuO<sub>4</sub>). The bottom-left inset is the magnified image of the selected region outlined by the dashed square. The upper-right inset is the FFT pattern of the selected region. g) Zoom-in TEM image of a  $DC_{60}$ -2TOF<sub>6</sub> colloidal particle (stained with RuO<sub>4</sub>). h) 1D small angle X-ray scattering pattern of  $DC_{60}$ -2TOF<sub>6</sub>. Relative peak ratios  $q/q^*$  (where the  $q^*$  is the location of primary peak) are indicated with arrows. The  $d$ -spacing corresponds to the primary peak is denoted as  $d_1$ . See Discussion 1.5 in the Supporting Information for details. i) 3D model of the detailed molecular packing in hexagonal columnar structure. The upper-right inset is the model for hexagonally arranged multiple-concentric loops. Only hydrophilic domains are displayed for clarity (red dashed square outlines the part being magnified for the detailed molecular packing). j) Internally structured colloidal morphology (red dashed square outlines the region corresponding to inset 1 and inset 2, respectively). The middle inset 1 demonstrates the mismatching region on corona. The right inset 2 demonstrates the columnar packing in the core. Scale bars, 200 nm (a, e), 100 nm (b–d, f), 50 nm (g), 20 nm (f, bottom-left inset).

d). Fast Fourier transform (FFT) imaging (Figure 4 f, upper-right inset) of a selected region further verifies the hexagonal features in reciprocal space. Given the higher electron density of DC<sub>60</sub> than OF rods after being stained, the dark spots and gray matrix should be attributed to DC<sub>60</sub> domains and OF rods, respectively. Small angle X-ray scattering (SAXS, Supporting Information, Figure S10) gives a relative peak ratio  $q/q^* = 1:\sqrt{3}:\sqrt{7}$  (where the  $q^*$  is the location of primary peak), indicating a hexagonal columnar inner structure (Supporting Information, Discussion 1.5). Continuous tilting TEM further confirms the suggested structure by monitoring the angular variation in reciprocal space (Supporting Information, Figure S11, and Discussion 1.6). Internally structured colloids are also revealed in a zoom-in TEM image of DC<sub>60</sub>-2TOF<sub>6</sub> after being stained (Figure 4g and Supporting Information, Figure S9e–h). Features including a double truncated conical shape and a hexagonal array of dark spots with a lamellar central region are observed. Tilting a colloid by 20° displays a key feature of spot-to-matrix transformation in hexagonally arranged multiple-concentric loops (Supporting Information, Figure S12).<sup>[35]</sup> The SAXS profile with relative peak ratio of 1: $\sqrt{3}$ :2: $\sqrt{7}$ :3 confirms this hexagonal columnar structure (Figure 4h and Supporting Information, Discussion 1.5). It should also be mentioned that, instead of forming hollow channels (as in the case of hexagonally packed hollow hoops<sup>[35]</sup>), the internal high-electron-density structures are filled with DC<sub>60</sub> due to the inner phase separation (Figure 4i). Self-assembly at a slower rate further suggests that an internally structured colloid is the thermodynamically favored morphology for DC<sub>60</sub>-2TOF<sub>6</sub> (Supporting Information, Figure S4b and Discussion 1.2). When the rod part is further elongated to DC<sub>60</sub>-2TOF<sub>8</sub>, the self-assembled structures still exhibit spherical colloidal morphologies (Figure 4d and Supporting Information, Figure S8d), whereas its inner ordered structures are hardly detected (Supporting Information, Figures S13). We note that DC<sub>60</sub>-2TOF<sub>4</sub> forms a hexagonally packed structure both in solution state and bulk state (Table 1). However, for DC<sub>60</sub>-2TOF<sub>6</sub>, the observed hexagonal structure in solution is different from the Frank–Kasper A15 phase in the bulk. This variation could be partly ascribed to the hydration of DC<sub>60</sub>, as suggested by diffusion-ordered NMR spectroscopy (DOSY) analysis (Supporting Information, Figure S14, Table S3, and Discussion 1.7), which increases the volume fraction of hydrophilic DC<sub>60</sub> and shifts the mesostructure from a spherical phase to a columnar phase.<sup>[36]</sup>

In the T-shape series, colloidal morphologies were observed when rods are elongated. Based on the calculation of packing parameters (as discussed in the following section, Table 1), longer tails ( $n_f > 2$ ) hinder the close packing of hydrophilic heads on corona, yielding a mismatching region ( $S_{\text{mismatch}}$ , inset 1 in Figure 4j) and highly unfavorable  $F_{\text{edge}}$  that destabilizes the system. Such an effect has rarely been observed in non-rigid block-copolymers.<sup>[8b]</sup> As a consequence, the colloids prefer adopting a non-spherical morphology (as the double truncated cones in DC<sub>60</sub>-2TOF<sub>6</sub>) to lower the  $F_{\text{bend}}$

**Table 1:** Summary of assembled structures and geometric parameters of giant lipids.

Samples	Structure (Solution)	Structure (Bulk) <sup>[a]</sup>	$M_{w,OF} [\text{kg mol}^{-1}]$ <sup>[a]</sup>	$l_t [\text{\AA}]$ <sup>[b]</sup>	$V_t l_t^{-1} [\text{nm}^2]$	$P$
DC <sub>60</sub> -2IOF <sub>2</sub>	Vesicle	LAM	0.841	21.5	1.40	0.792
DC <sub>60</sub> -2IOF <sub>4</sub>	Vesicle	LAM	1.51	39.5	1.36	0.774
DC <sub>60</sub> -2IOF <sub>6</sub>	Nanosheet	LAM	2.16	52.4	1.47	0.835
DC <sub>60</sub> -2IOF <sub>8</sub>	Nanosheet	LAM	2.83	75.4	1.34	0.760
DC <sub>60</sub> -2TOF <sub>2</sub>	Vesicle	LAM	0.872	15.7	1.98	1.12
DC <sub>60</sub> -2TOF <sub>4</sub>	Colloidal Particle	HEX	1.54	12.2	4.46	2.53
DC <sub>60</sub> -2TOF <sub>6</sub>	Colloidal Particle	A15	2.20	12.2	6.45	3.66
DC <sub>60</sub> -2TOF <sub>8</sub>	Colloidal Particle	BCC	2.86	12.2	8.40	4.76

[a] These data were reported in our previous work.<sup>[24]</sup> LAM, HEX, A15, and BCC represent lamellar, hexagonal, Frank–Kasper A15, and body-centered cubic mesostructures, respectively. [b] Entries 1–5 are estimated from AFM height profile; Entries 6–8 are estimated from the short axis of OF tail (Supporting Information, Discussion 1.3).

on the surface. Over the course of elongating the rod length, the morphological evolution from vesicles to colloids (assuming the two morphologies have identical surface curvature, spherical volume, and coronal composition) could be qualitatively rationalized since the colloids significantly decrease the  $F_{\text{edge}}$  by lowering the average surface area accessible to each molecules in assemblies and eliminating the inner surface. Such compensation from  $F_{\text{edge}}$  is sufficient to stabilize the system based on our experimental observation even though an extra energetic term ( $F_{\text{coral}}$ ) should emerge from both elastic free energy and entropic term of mixing two incommensurate parts inside the core part.<sup>[37]</sup> This  $F_{\text{coral}}$  term could be minimized by internal phase separation (inset 2 in Figure 4j) under the boundary condition confined by colloidal surface geometry and domain size of periodic structures, which has been predicted and studied in other studies.<sup>[38]</sup>

### Geometric Effects in a Magnified Lipid-like System

The driving force of forming different assembled structures induced by I-shape and T-shape giant lipids can be rationalized by the argument of their shape. From a geometric aspect, packing parameter ( $P$ ) of amphiphilic molecules is characterized by [Eq. (3)]:<sup>[39]</sup>

$$P = V_t l_t^{-1} / a_h \quad (3)$$

where  $a_h$  is the equilibrium interfacial area of the hydrophilic head, and  $V_t$  and  $l_t$  are the volume and length of hydrophobic tails, respectively. The volume of two OF tails could be calculated by  $V_t = 2 M_w / N_A \rho$ , where  $M_w$  and  $\rho$  are the molecular weight and density of one OF tail, and  $N_A$  is the Avogadro's number.

Since the chemical structures of giant lipids are precisely defined, we are able to quantitatively calculate the  $P$  values for both series and summarize them in Table 1 (a detailed calculation is presented in Discussion 1.3 in the Supporting Information). When the value of  $P$  ranges from 0.5 to 1, bilayered structures with spontaneous curvature (for example, vesicles) are more favorable.<sup>[39a]</sup> In the I-shape series, the  $P$  values of all giant lipids are in this range, consistent with our experimental observations of vesicular morphologies for  $DC_{60}$ -2IOF<sub>2</sub> and  $DC_{60}$ -2IOF<sub>4</sub> (Figure 2 a,b). When the OF tail gets longer, the formation of 2D nanosheets rather than vesicles formed by  $DC_{60}$ -2IOF<sub>6</sub> and  $DC_{60}$ -2IOF<sub>8</sub> can be attributed to the drastic increase in bending energy, as we discuss above. For the T-shape series,  $P$  increases with the elongation of OF tails. For  $DC_{60}$ -2TOF<sub>2</sub>, though the value of  $P$  slightly exceeds 1, the tilting-up conformation of OF tails allows the maintenance of its vesicular structure. When the  $n_f$  increases to 4 and 6,  $P$  reaches 2.53 and 3.66, respectively. The higher  $P$  necessitates higher curvature to settle the unmatched interfacial region as in the case of  $DC_{60}$ -2TOF<sub>4</sub> and  $DC_{60}$ -2TOF<sub>6</sub>.

As a prototype study, I-shape and T-shape giant lipids are designed to evaluate the effects of head–tail ratio and cross-sectional area, respectively. In a comparable region of head–tail ratio, giant lipids recast the phase behavior of their small molecular analogues to a certain degree. Linear lipids form bilayered vesicles without morphological variation, when the carbon number varies from 10 to 24.<sup>[18]</sup> Theoretical investigation also supports that the chain length only influences the vesicle radius.<sup>[40]</sup> With a similar head–tail ratio, giant lipids form bilayered vesicles as well (natural lipid glucosylceramide whose carbon number is 16 the closest head–tail ratio to that of  $DC_{60}$ -2IOF<sub>2</sub>, Supporting Information, Figure S15). Furthermore, both lipidic and giant lipidic systems demonstrate that membrane thickness is proportional to the number of repeating tail units, indicating the presence of fully extended tails. On the other hand, branched acyl chains with larger cross-sectional area facilitate the formation of form inverted phases.<sup>[41]</sup> This non-bilayer propensity observed in small molecules is also presented in T-shape giant lipids. Due to the small feature size and weak contrast of electron density, it is challenging to directly observe the inverted phase of lipids by electron microscopy. In contrast, giant lipids provide a versatile platform for exploring the aggregation mode of these inverted phases. Moreover, compared with lipids, giant lipids offer a wider window in tuning the head–tail ratio and cross-sectional area, and thus present a rich variety of assembling structures. Finally, benefiting from the systematic study of sphere-coil giant surfactants (hydrophilic  $C_{60}$  tethered by two polystyrene tails, namely,  $AC_{60}$ -2PS<sub>n</sub>),<sup>[19a]</sup> it is of significant importance to assess the impact of tail rigidity on self-assembly. For  $AC_{60}$ -2PS<sub>n</sub>, bilayered vesicles were observed independent of the tail length, whereas a phase transition from vesicles to 2D nanosheets is observed for  $DC_{60}$ -2IOF<sub>n</sub> with increasing OF tail length. The morphological variation between sphere-coil and sphere-rod can be ascribed to a drastic increase in bending energy associated with the higher rigidity of OF tails.

## Conclusion

We have demonstrated our prototype self-assembly study of I-shape and T-shape giant lipids. They are specifically designed to evaluate the effects of head–tail ratio and cross-sectional area while assembling as in the case of linear and branched natural lipids. Mandated by these two parameters, I-shape giant lipids exhibit completely distinct self-assembly behaviors from their T-shape topological isomers. With increasing the OF tail length, a morphological variation from bilayered vesicles to interdigitated 2D nanosheets is observed in I-shape giant lipids, and regulated by a delicate balance of edge energy and bending energy. The formation of colloidal particles is prevalently observed in T-shape analogues due to their mismatched cross-sectional area between hydrophilic head and hydrophobic tails. Compared with the self-assembly of natural lipids, they share common features in constructing bilayered vesicles, while forming various morphologies when geometric parameters are modified. Giant lipids, which feature a head–tail configuration, monodispersed molecular weight, and minor interpenetration of rod-like tails, not only offer a prototype for understanding the self-assembly principles of natural lipids from a magnified dimension, but may also be suitable building blocks to construct artificial organelles that could mimic dynamic biological processes.

## Acknowledgements

We thank Dr. Liubin Feng from the High-field Nuclear Magnetic Resonance Research Center, Xiamen University and Dr. Nan Zheng from the State Key Laboratory of Luminescent Materials and Devices, South China University of Technology, Dr. Jing Wang from the South China Advanced Institute for Soft Matter Science and Technology, South China University of Technology for their technical supports. We thank Prof. Mingjun Huang, Dr. Hao Su, Dr. Qi Xiao, Dr. Ru-Qiang Lu, and Prof. Xiao-Yu Cao for helpful discussions. This work was supported by the National Science Foundation (DMR-1408872 to S.Z.D.C., CHE-1904397 to T.L.), the Introduced Innovative R&D Team Project of “The Pearl River Talent Recruitment Program” of Guangdong Province (no. 2016ZT06C322), the National Natural Science Foundation of China (U1832220 to S.Z.D.C.). We thank technical support from Shanghai Synchrotron Radiation Facility (SSRF).

## Conflict of interest

The authors declare no conflict of interest.

**Keywords:** amphiphiles · biomimetic synthesis · membranes · oligofluorene · supramolecular chemistry

**How to cite:** *Angew. Chem. Int. Ed.* **2020**, *59*, 5226–5234  
*Angew. Chem.* **2020**, *132*, 5264–5272

[1] a) J. J. Stezowski, K. H. Jogun, E. Eckle, K. Bartels, *Nature* **1978**, 274, 617; b) V. Percec, A. E. Dulcey, V. S. Balagurusamy, Y. Miura, J. Smidrkal, M. Peterca, S. Nummelin, U. Edlund, S. D. Hudson, P. A. Heiney, H. Duan, S. N. Magonov, S. A. Vinogradov, *Nature* **2004**, 430, 764; c) Y. Tu, F. Peng, A. Adawy, Y. Men, L. K. Abdelmohsen, D. A. Wilson, *Chem. Rev.* **2016**, 116, 2023.

[2] a) M. Li, R. L. Harbron, J. V. M. Weaver, B. P. Binks, S. Mann, *Nat. Chem.* **2013**, 5, 529; b) W. Abuillan, A. S. Becker, B. Deme, T. Homma, H. Isobe, K. Harano, E. Nakamura, M. Tanaka, *J. Am. Chem. Soc.* **2018**, 140, 11261.

[3] a) M. Weiss, J. P. Frohnmayr, L. T. Benk, B. Haller, J. W. Janiesch, T. Heitkamp, M. Borsch, R. B. Lira, R. Dimova, R. Lipowsky, E. Bodenschatz, J. C. Baret, T. Vidakovic-Koch, K. Sundmacher, I. Platzman, J. P. Spatz, *Nat. Mater.* **2018**, 17, 89; b) B. M. Discher, H. Bermudez, D. A. Hammer, D. E. Discher, Y.-Y. Won, F. S. Bates, *J. Phys. Chem. B* **2002**, 106, 2848.

[4] a) Q. Xiao, A. K. Ludwig, C. Romano, I. Buzzacchera, S. E. Sherman, M. Vetro, S. Vertes, H. Kaltner, E. H. Reed, M. Moller, C. J. Wilson, D. A. Hammer, S. Oscarson, M. L. Klein, H. J. Gabius, V. Percec, *Proc. Natl. Acad. Sci. USA* **2018**, 115, E2509; b) C. Rodriguez-Emmenegger, Q. Xiao, N. Y. Kostina, S. E. Sherman, K. Rahimi, B. E. Partridge, S. Li, D. Sahoo, A. M. Reveron Perez, I. Buzzacchera, H. Han, M. Kerzner, I. Malhotra, M. Moller, C. J. Wilson, M. C. Good, M. Goulian, T. Baumgart, M. L. Klein, V. Percec, *Proc. Natl. Acad. Sci. USA* **2019**, 116, 5376; c) A. K. Ludwig, M. Michalak, Q. Xiao, U. Gilles, F. J. Medrano, H. Ma, F. G. Fitzgerald, W. D. Hasley, A. Melendez-Davila, M. Liu, K. Rahimi, N. Y. Kostina, C. Rodriguez-Emmenegger, M. Moller, I. Lindner, H. Kaltner, M. Cudic, D. Reusch, J. Kopitz, A. Romero, S. Oscarson, M. L. Klein, H. J. Gabius, V. Percec, *Proc. Natl. Acad. Sci. USA* **2019**, 116, 2837.

[5] a) M. Kumar, M. Grzelakowski, J. Zilles, M. Clark, W. Meier, *Proc. Natl. Acad. Sci. USA* **2007**, 104, 20719; b) V. Percec, D. A. Wilson, P. Leowanawat, C. J. Wilson, A. D. Hughes, M. S. Kaucher, D. A. Hammer, D. H. Levine, A. J. Kim, F. S. Bates, K. P. Davis, T. P. Lodge, M. L. Klein, R. H. DeVane, E. Aqad, B. M. Rosen, A. O. Argintaru, M. J. Sienkowska, K. Rissanen, S. Nummelin, J. Ropponen, *Science* **2010**, 328, 1009.

[6] a) B. M. Discher, Y. Y. Won, D. S. Ege, J. C. Lee, F. S. Bates, D. E. Discher, D. A. Hammer, *Science* **1999**, 284, 1143; b) Y. Mai, A. Eisenberg, *Chem. Soc. Rev.* **2012**, 41, 5969.

[7] a) M. Peterca, V. Percec, P. Leowanawat, A. Bertin, *J. Am. Chem. Soc.* **2011**, 133, 20507; b) V. Percec, P. Leowanawat, H.-J. Sun, O. Kulikov, C. D. Nusbaum, T. M. Tran, A. Bertin, D. A. Wilson, M. Peterca, S. Zhang, N. P. Kamat, K. Vargo, D. Moock, E. D. Johnston, D. A. Hammer, D. J. Pochan, Y. Chen, Y. M. Chabre, T. C. Shiao, M. Bergeron-Brlek, S. André, R. Roy, H.-J. Gabius, P. A. Heiney, *J. Am. Chem. Soc.* **2013**, 135, 9055; c) S. Zhang, Q. Xiao, S. E. Sherman, A. Muncan, A. D. M. Ramos Vicente, Z. Wang, D. A. Hammer, D. Williams, Y. Chen, D. J. Pochan, S. Vértesy, S. André, M. L. Klein, H.-J. Gabius, V. Percec, *J. Am. Chem. Soc.* **2015**, 137, 13334; d) Q. Xiao, S. Zhang, Z. Wang, S. E. Sherman, R.-O. Moussodia, M. Peterca, A. Muncan, D. R. Williams, D. A. Hammer, S. Vértesy, S. André, H.-J. Gabius, M. L. Klein, V. Percec, *Proc. Natl. Acad. Sci. USA* **2016**, 113, 1162.

[8] a) Z. Lin, J. Sun, Y. Zhou, Y. Wang, H. Xu, X. Yang, H. Su, H. Cui, T. Aida, W. Zhang, S. Z. D. Cheng, *J. Am. Chem. Soc.* **2017**, 139, 5883; b) X. Yu, K. Yue, I. F. Hsieh, Y. Li, X. H. Dong, C. Liu, Y. Xin, H. F. Wang, A. C. Shi, G. R. Newkome, R. M. Ho, E. Q. Chen, W. B. Zhang, S. Z. D. Cheng, *Proc. Natl. Acad. Sci. USA* **2013**, 110, 10078.

[9] a) K. B. Vargo, R. Parthasarathy, D. A. Hammer, *Proc. Natl. Acad. Sci. USA* **2012**, 109, 11657; b) M. C. Huber, A. Schreiber, P. von Olshausen, B. R. Varga, O. Kretz, B. Joch, S. Barnert, R. Schubert, S. Eimer, P. Kele, S. M. Schiller, *Nat. Mater.* **2015**, 14, 125.

[10] a) H. Dou, M. Li, Y. Qiao, R. Harniman, X. Li, C. E. Boott, S. Mann, I. Manners, *Nat. Commun.* **2017**, 8, 426; b) B. Y. Guan, L. Yu, X. W. Lou, *Adv. Mater.* **2016**, 28, 9596.

[11] a) R. M. Gorgoll, K. Harano, E. Nakamura, *J. Am. Chem. Soc.* **2016**, 138, 9675; b) R. M. Gorgoll, T. Tsubota, K. Harano, E. Nakamura, *J. Am. Chem. Soc.* **2015**, 137, 7568; c) S. Zhou, C. Burger, B. Chu, M. Sawamura, N. Nagahama, M. Togano, U. E. Hackler, H. Isobe, E. Nakamura, *Science* **2001**, 291, 1944.

[12] a) S. E. Sherman, Q. Xiao, V. Percec, *Chem. Rev.* **2017**, 117, 6538; b) H. Ringsdorf, B. Schlarb, J. Venzmer, *Angew. Chem. Int. Ed. Engl.* **1988**, 27, 113; *Angew. Chem.* **1988**, 100, 117; c) T. Kunitake, *Angew. Chem. Int. Ed. Engl.* **1992**, 31, 709; *Angew. Chem.* **1992**, 104, 692; d) J. L. Thomas, D. A. Tirrell, *Acc. Chem. Res.* **1992**, 25, 336.

[13] a) M. R. Molla, P. Rangadurai, L. Antony, S. Swaminathan, J. J. de Pablo, S. Thayumanavan, *Nat. Chem.* **2018**, 10, 659; b) P. G. van Rhee, R. S. Rikken, L. K. Abdelmohsen, J. C. Maan, R. J. Nolte, J. C. van Hest, P. C. Christianen, D. A. Wilson, *Nat. Commun.* **2014**, 5, 5010; c) T. Yu, X. Liu, A. L. Bolcato-Bellemin, Y. Wang, C. Liu, P. Erbacher, F. Qu, P. Rocchi, J. P. Behr, L. Peng, *Angew. Chem. Int. Ed.* **2012**, 51, 8478; *Angew. Chem.* **2012**, 124, 8606; d) S. Nummelin, V. Liljestrom, E. Saarikoski, J. Ropponen, A. Nykanen, V. Linko, J. Seppala, J. Hirvonen, O. Ikkala, L. M. Bimbo, M. A. Kostiainen, *Chem. Eur. J.* **2015**, 21, 14433.

[14] a) S.-Y. Li, W.-X. Qiu, H. Cheng, F. Gao, F.-Y. Cao, X.-Z. Zhang, *Adv. Funct. Mater.* **2017**, 27, 1604916; b) K. Yang, Y. Liu, Y. Liu, Q. Zhang, C. Kong, C. Yi, Z. Zhou, Z. Wang, G. Zhang, Y. Zhang, N. M. Khashab, X. Chen, Z. Nie, *J. Am. Chem. Soc.* **2018**, 140, 4666; c) M. Filippi, D. Patrucco, J. Martinelli, M. Botta, P. Castro-Hartmann, L. Tei, E. Terreno, *Nanoscale* **2015**, 7, 12943.

[15] a) B. V. V. S. P. Kumar, A. J. Patil, S. Mann, *Nat. Chem.* **2018**, 10, 1154; b) P. Gobbo, A. J. Patil, M. Li, R. Harniman, W. H. Briscoe, S. Mann, *Nat. Mater.* **2018**, 17, 1145; c) V. Noireaux, Y. T. Maeda, A. Libchaber, *Proc. Natl. Acad. Sci. USA* **2011**, 108, 3473.

[16] a) R. J. Pace, S. I. Chan, *J. Chem. Phys.* **1982**, 76, 4241; b) J. C. Owicki, M. W. Springgate, H. M. McConnell, *Proc. Natl. Acad. Sci. USA* **1978**, 75, 1616.

[17] P. K. J. Kinnunen, *Chem. Phys. Lipids* **1991**, 57, 375.

[18] B. A. Lewis, D. M. Engelman, *J. Mol. Biol.* **1983**, 166, 211.

[19] a) X. Yu, W. B. Zhang, K. Yue, X. Li, H. Liu, Y. Xin, C. L. Wang, C. Wesdemiotis, S. Z. D. Cheng, *J. Am. Chem. Soc.* **2012**, 134, 7780; b) X. Yu, S. Zhong, X. Li, Y. Tu, S. Yang, R. M. Van Horn, C. Ni, D. J. Pochan, R. P. Quirk, C. Wesdemiotis, W. B. Zhang, S. Z. D. Cheng, *J. Am. Chem. Soc.* **2010**, 132, 16741.

[20] a) B. Ni, H. Qu, J. Mao, R. Bai, S. Zhang, X. Feng, C. Wesdemiotis, X.-H. Dong, S. Z. D. Cheng, *Polymer* **2019**, 167, 118; b) R. Zhang, X. Feng, R. Zhang, W. Shan, Z. Su, J. Mao, C. Wesdemiotis, J. Huang, X. Y. Yan, T. Liu, T. Li, M. Huang, Z. Lin, A. C. Shi, S. Z. D. Cheng, *Angew. Chem. Int. Ed.* **2019**, 58, 11879–11885; *Angew. Chem.* **2019**, 131, 12005–12011.

[21] a) M. Huang, C. H. Hsu, J. Wang, S. Mei, X. Dong, Y. Li, M. Li, H. Liu, W. Zhang, T. Aida, W. B. Zhang, K. Yue, S. Z. D. Cheng, *Science* **2015**, 348, 424; b) H. Liu, C. H. Hsu, Z. Lin, W. Shan, J. Wang, J. Jiang, M. Huang, B. Lotz, X. Yu, W. B. Zhang, K. Yue, S. Z. D. Cheng, *J. Am. Chem. Soc.* **2014**, 136, 10691; c) B. Ni, M. Huang, Z. Chen, Y. Chen, C. H. Hsu, Y. Li, D. Pochan, W. B. Zhang, S. Z. D. Cheng, X. H. Dong, *J. Am. Chem. Soc.* **2015**, 137, 1392; d) W. Zhang, M. Huang, H. Su, S. Zhang, K. Yue, X. H. Dong, X. Li, H. Liu, S. Zhang, C. Wesdemiotis, B. Lotz, W. B. Zhang, Y. Li, S. Z. D. Cheng, *ACS Cent. Sci.* **2016**, 2, 48; e) Z. Su, C. H. Hsu, Z. Gong, X. Feng, J. Huang, R. Zhang, Y. Wang, J. Mao, C. Wesdemiotis, T. Li, S. Seifert, W. Zhang, T. Aida, M. Huang, S. Z. D. Cheng, *Nat. Chem.* **2019**, 11, 899.

[22] a) H. J. Sun, S. Zhang, V. Percec, *Chem. Soc. Rev.* **2015**, *44*, 3900; b) "Hierarchical Macromolecular Structures: 60 Years after the Staudinger Nobel Prize I": V. Percec in *Advances in Polymer Science*, Vol. 261 (Ed.: V. Percec), Springer, Cham, **2013**, pp. 173–197; c) F. Würthner, C. R. Saha-Moller, B. Fimmel, S. Ogi, P. Leowanawat, D. Schmidt, *Chem. Rev.* **2016**, *116*, 962; d) H. Nitta, K. Harano, M. Isomura, E. H. G. Backus, M. Bonn, E. Nakamura, *J. Am. Chem. Soc.* **2017**, *139*, 7677; e) P. Bairi, K. Minami, J. P. Hill, W. Nakanishi, L. K. Shrestha, C. Liu, K. Harano, E. Nakamura, K. Ariga, *ACS Nano* **2016**, *10*, 8796; f) J. Zhang, Y. F. Song, L. Cronin, T. Liu, *J. Am. Chem. Soc.* **2008**, *130*, 14408.

[23] X. Feng, R. Zhang, Y. Li, Y. L. Hong, D. Guo, K. Lang, K. Y. Wu, M. Huang, J. Mao, C. Wesdemiotis, Y. Nishiyama, W. Zhang, W. Zhang, T. Miyoshi, T. Li, S. Z. D. Cheng, *ACS Cent. Sci.* **2017**, *3*, 860.

[24] Z. Lin, X. Yang, H. Xu, T. Sakurai, W. Matsuda, S. Seki, Y. Zhou, J. Sun, K. Y. Wu, X. Y. Yan, R. Zhang, M. Huang, J. Mao, C. Wesdemiotis, T. Aida, W. Zhang, S. Z. D. Cheng, *J. Am. Chem. Soc.* **2017**, *139*, 18616.

[25] S. Zhang, H. J. Sun, A. D. Hughes, R. O. Moussodia, A. Bertin, Y. Chen, D. J. Pochan, P. A. Heiney, M. L. Klein, V. Percec, *Proc. Natl. Acad. Sci. USA* **2014**, *111*, 9058.

[26] S. W. Provencher, *Comput. Phys. Commun.* **1982**, *27*, 229.

[27] P. C. Hiemenz, R. Rajagopalan, *Principles of Colloid and Surface Chemistry*, 3rd ed., Marcel Dekker, New York, **1997**, pp. 193–242.

[28] a) E. A. Evans, *Biophys. J.* **1974**, *14*, 923; b) F. Jülicher, R. Lipowsky, *Phys. Rev. Lett.* **1993**, *70*, 2964; c) W. T. Góźdż, G. Gompper, *Phys. Rev. Lett.* **1998**, *80*, 4213; d) X. Li, M. M. Denn, *Phys. Rev. Lett.* **2001**, *86*, 656; e) D. Cholakova, N. Denkov, S. Tcholakova, Z. Valkova, S. K. Smoukov, *Langmuir* **2019**, *35*, 5484; f) Z. Shen, H. Ye, M. Kroger, Y. Li, *Nanoscale* **2018**, *10*, 4545; g) L. Chen, X. Li, Y. Zhang, T. Chen, S. Xiao, H. Liang, *Nanoscale* **2018**, *10*, 11969.

[29] a) W. Helfrich, *Z. Naturforsch. C* **1973**, *28*, 693; b) E. A. Evans, R. Skalak, *Mechanics and Thermodynamics of Biomembranes*, CRC, New York, **1980**, pp. 112–117.

[30] W. Rawicz, K. C. Olbrich, T. McIntosh, D. Needham, E. Evans, *Biophys. J.* **2000**, *79*, 328.

[31] a) L. A. Girifalco, R. J. Good, *J. Phys. Chem.* **1957**, *61*, 904; b) L. Gránásy, M. Tegze, A. Ludwig, *Mater. Sci. Eng. A* **1991**, *133*, 577.

[32] M. Antonietti, S. Förster, *Adv. Mater.* **2003**, *15*, 1323.

[33] a) E. Helfand, Z. R. Wasserman, *Macromolecules* **1976**, *9*, 879; b) F. S. Bates, G. H. Fredrickson, *Annu. Rev. Phys. Chem.* **1990**, *41*, 525.

[34] a) C. Sinturel, F. S. Bates, M. A. Hillmyer, *ACS Macro Lett.* **2015**, *4*, 1044; b) R. A. Orwoll, P. A. Arnold, *Physical Properties of Polymers Handbook*, Springer, New York, **2007**, pp. 233–257.

[35] L. Zhang, C. Bartels, Y. Yu, H. Shen, A. Eisenberg, *Phys. Rev. Lett.* **1997**, *79*, 5034.

[36] A. K. Khandpur, S. Förster, F. S. Bates, I. W. Hamley, A. J. Ryan, W. Bras, K. Almdal, K. Mortensen, *Macromolecules* **1995**, *28*, 8796.

[37] a) E. B. Zhulina, M. Adam, I. LaRue, S. S. Sheiko, M. Rubinstein, *Macromolecules* **2005**, *38*, 5330; b) E. B. Zhulina, O. V. Borisov, *Macromolecules* **2012**, *45*, 4429.

[38] a) B. Yu, B. Li, Q. Jin, D. Ding, A.-C. Shi, *Macromolecules* **2007**, *40*, 9133; b) P. Chen, H. Liang, A.-C. Shi, *Macromolecules* **2008**, *41*, 8938; c) P. Chi, Z. Wang, B. Li, A.-C. Shi, *Langmuir* **2011**, *27*, 11683.

[39] a) J. N. Israelachvili, D. J. Mitchell, B. W. Ninham, *J. Chem. Soc. Faraday Trans.* **1976**, *72*, 1525; b) X. Yu, Y. Li, X.-H. Dong, K. Yue, Z. Lin, X. Feng, M. Huang, W.-B. Zhang, S. Z. D. Cheng, *J. Polym. Sci. Part B* **2014**, *52*, 1309.

[40] J. N. Israelachvili, D. J. Mitchell, B. W. Ninham, *Biochim. Biophys. Acta Biomembr.* **1977**, *470*, 185.

[41] R. M. Epand, R. F. Epand, A. Decicco, D. Schwarz, *Eur. J. Biochem.* **2000**, *267*, 2909.

Manuscript received: December 16, 2019

Accepted manuscript online: January 20, 2020

Version of record online: February 12, 2020